(12)

ANALYSIS OF THE MULTIPATH
ENVIRONMENT FOR APATS TESTING

By

G.A. ROBERTSHAW

NOVEMBER 1981

DTIC
SELE
JAN 1 1 1982
E

Prepared for

DEPUTY FOR SURVEILLANCE AND CONTROL SYSTEMS
ELECTRONIC SYSTEMS DIVISION
AIR FORCE SYSTEMS COMMAND
UNITED STATES AIR FORCE
Hanscom Air Force Base, Massachusetts

(12) 51

AD A109345

DTIC FILE COPY

235 05C 82 01

REVIEW AND APPROVAL

This technical report has been reviewed and is approved for publication.

(Signature) GS-13
Michael Zymaris
Project Engineer/Scientist

FOR THE COMMANDER

(Signature) Lt Col, USAF, NPMB
EDWIN C. DOBROWSKI, Lt Col, USAF, NPMB
System Program Director, APATS

REPORT DOCUMENTATION PAGE		READ INSTRUCTIONS BEFORE COMPLETING FORM
1. REPORT NUMBER ESD-TR-81-254	2. GOVT ACCESSION NO. AD-A109345	3. RECIPIENT'S CATALOG NUMBER
4. TITLE *(and Subtitle)* ANALYSIS OF THE MULIPATH ENVIRONMENT FOR APATS TESTING		5. TYPE OF REPORT & PERIOD COVERED
		6. PERFORMING ORG. REPORT NUMBER MTR-8391
7. AUTHOR(s) G. A. ROBERTSHAW		8. CONTRACT OR GRANT NUMBER(s) F19628-81-C-0001
9. PERFORMING ORGANIZATION NAME AND ADDRESS The MITRE Corporation P.O. Box 208 Bedford, MA 01730		10. PROGRAM ELEMENT, PROJECT, TASK AREA & WORK UNIT NUMBERS Project No. 4290
11. CONTROLLING OFFICE NAME AND ADDRESS Deputy for surveillance and Control Systems		12. REPORT DATE November 1981
Electronic Systems Division, AFSC Hanscom Air Force Base, MA 01730		13. NUMBER OF PAGES 52
14. MONITORING AGENCY NAME & ADDRESS(*if different from Controlling Office*)		15. SECURITY CLASS. *(of this report)* UNCLASSIFIED
		15a. DECLASSIFICATION/DOWNGRADING SCHEDULE

16. DISTRIBUTION STATEMENT *(of this Report)*

Approved for public release; distribution unlimited

17. DISTRIBUTION STATEMENT *(of the abstract entered in Block 20, if different from Report)*

18. SUPPLEMENTARY NOTES

19. KEY WORDS *(Continue on reverse side if necessary and identify by block number)*

APATS
APATS TEST
MULTIPATH
PROPAGATION

Active Phased Array Interrogating System

20. ABSTRACT *(Continue on reverse side if necessary and identify by block number)* Phase II of the APATS test program will include tower-air-ground (TAG) testing of system sensitivity, tracking capability, and other functions. As presently envisioned, these test configurations involve propagation paths for which transmitter and receiver (APATS) heights are small relative to baseline separations and interference caused by multipath propagation must be considered in the context of the test objectives. A two-path propagation model which incorporates specular reflection from the earth is developed and calculations are performed

(over)

DD `FORM 1 JAN 73` 1473

20. (Concluded)

for typical test configurations. The anticipated effects and ramifications of multi-path interference are discussed and specific test configurations are recommended.

ACKNOWLEDGMENTS

Accession For		
NTIS GRA&I		☒
DTIC TAB		☐
Unannounced		☐
Justification		
By		
Distribution/		
Availability Codes		
Dist	Avail and/or Special	
A		

TABLE OF CONTENTS

LIST OF ILLUSTRATIONS

LIST OF TABLES

SECTION 1

INTRODUCTION AND CONCLUSIONS

Phase II of the APATS (ARIA Phased Array Telemetry System) test
program, as currently envisioned, will include tower-air-ground
(TAG) testing to be performed at Wright-Patterson AFB, Dayton, Ohio.
These tests will be performed with the ARIA stationary and with one
or more transmitters (stationary or moving) within the APATS field
of view. APATS is required to acquire and track up to 8 source
signals (2 per re-entry vehicle) without appreciable degradation due
to any APATS processing function, such as, for example, beam
steering. The sensitivity of APATS will also be tested, either by
absolute measurements or by calibration against the known
sensitivity of the existing 2.1 m parabolic dish antenna on the ARIA
nose.

Test configurations under consideration include:

(1) APATS sensitivity measurements employing the simulation
antenna mounted on the existing 24.25m (80ft.)tower with
the ARIA approximately 400 m away on the operational
apron.

(2) APATS tracking exercises for which sources are carried
upon light vehicles which can move freely within the APATS
field of view.

In both of these cases the configuration geometries incur
propagation paths which are nearly parallel to relatively flat
ground. Under these circumstances, interference from a strongly
reflected surface wave is anticipated. This type of multipath

1

interference can be greatly ameliorated by rejecting these test configurations and employing sources lofted by aircraft, balloons or specially errected towers which can place the sources at significantly larger elevation angles ($\sim15^{\circ}$ or more) with respect to the ARIA antennas. These geometries permit substantial reduction of the reflected signal by the APATS antenna directivity. On the other hand, if test configurations 1 and 2 are adequate, in spite of multipath propagation, they should incur less time and expense to perform than the alternative ethods.

The primary purpose of this study is to ascertain the character and severity of multipath interference for test configurations 1 and 2 above, in order to determine the conditions under which test objectives may be met, or if these objectives are feasible. As a spin-off of this analysis, several attractive test configurations which should be relatively immune to multipath degradation are suggested and discussed.

The conclusions of this study are summarized as follows:

(1) The existing antenna mounted on the 24.25m tower cannot be used to perform accurate sensitivity measurements unless the baseline distance between the tower and APATS can be reduced to a fraction of the 400 m limit imposed by the configuration of the tower and operational apron. Rough calibration (±3 dB) should be feasible however.

(2) Sources mounted upon light ground vehicles can be employed to test the APATS tracking capability if baseline distances between 100m and 150m are maintained. This test scenario, however, will not test APATS tracking in elevation due to the planar propagation geometry.

2

Other test configurations which have merit and are not subject to serious multipath degradation include:

(1) An elevated vertically polarized source antenna configured such that the specular transmission between the source and APATS occurs at grazing angles in the vicinity of the Fresnel coefficient minimum. The incidence angle at which the minimum occurs is a function of the surface conductivity and relative dielectric constant. The required baselines and heights (See Fig.1) necessary to implement this optimum configuration are given in Tables 1 and 2 for grazing angles of 17.5° and 10.5°, which are appropriate for average land and moist earth, respectively.

(2) Any configuration which places the source transmitter in the far field of the receiving antenna at an elevation relative to the mean ground surface of 15° or greater should be suitable for testing.

(3) A test configuration which utilizes a "windmill" type source antenna support with antennas attached to the ends of one or two (orthogonal) arms would be particularly advantageous, since it would enable simultaneous tracking of multiple sources in both elevation and azimuth to be tested. If linearly polarized antennas were used for sources, the APATS polarization diversity capability would also be exercised, since the plane of polarization of a source would rotate with the arms along the circular trajectory.

(4) APATS testing can be accomplished using light aircraft, helicopters, or balloons to loft the transmitting

3

TABLE 1

**Optimum APATS-Source Geometries
Over Average Land ($\theta_B = 17.5°$)**

$\dfrac{h_r}{D}$	1m	2m	3m	4m
60m	h_s=17.2m B= 57.7m	16.3 58.1	15.4 58.3	14.4 58.4
80m	23.2 76.8	22.4 77.2	21.4 77.5	20.5 77.7
100m	29.2 95.9	28.4 96.3	27.5 96.7	26.6 97.0

TABLE 2

**Optimum APATS-Source Geometries
Over Moist Earth ($\theta_B = 10.5°$)**

$\dfrac{h_r}{D}$	1m	2m	3m	4m
60m	h_s=10.0m B= 59.2m	8.9 58.9	7.8 58.3	6.6 57.3
80m	13.6 78.9	12.6 78.8	11.5 78.4	10.4 77.8
100m	17.3 98.6	16.3 98.6	15.2 98.4	14.1 97.9

4

packages; however, these alternatives may be expensive or
inconvenient compared to testing performed with ground
apparatus only.

In Section 2, the multipath propagation model developed specifically
for the TAG test environment is presented, while in Section 3 the
results of calculations based on the model are discussed for several
hypothetical test configurations. Section 3, which is subdivided by
configuration or test environment, contains more detailed
discussions and justifications for the conclusions briefly reported
here.

SECTION 2

MULTIPATH MODEL

2.1 BASIC CONSIDERATIONS

When the ARIA is located on the ground, its telemetry antennas, i.e., both the proposed APATS antenna and existing 2.1m parabolic dish antenna in the nose, lie between heights of 1m and 5m. For simplicity it will be assumed that both antenna apertures lie in a vertical plane (horizontal boresights) and that the test transmitters are in the vertical plane which includes the array antenna boresight at a separation B (baseline) measured along the intervening ground. A typical test configuration which employs a test source close to the ground is illustrated in Figure 1. The analysis developed below will permit the determination of the amplitude and phase variation across the array and dish aperture in the presence of multipath interference.

The distance between the source and array must be sufficiently large to ensure that the source is in the far (Fraunhofer) field of the antenna. The range, R, of the source must therefore satisfy,[1]

$$R > \frac{2A^2}{\lambda} \tag{1}$$

in which A is the width of the array aperture and λ is the electromagnetic wavelength. For an array antenna 2m x 2m (approximate APATS antenna size) at S-band (λ = 13.3 cm) the range of the source must exceed 60m; however, conservative engineering practice suggests that larger separations should be employed '. practical.[2]
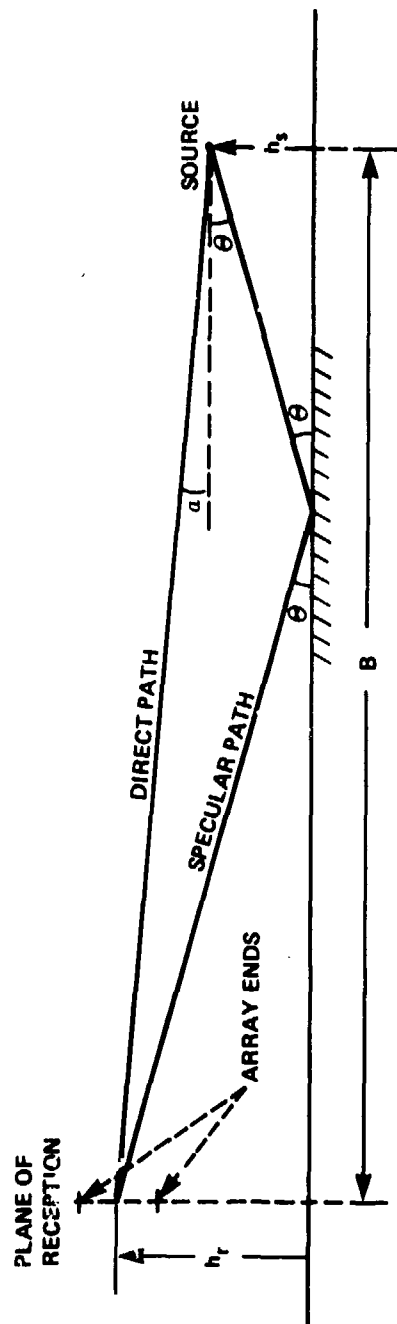
7

Figure 1. GROUND TEST MULTIPATH GEOMETRY
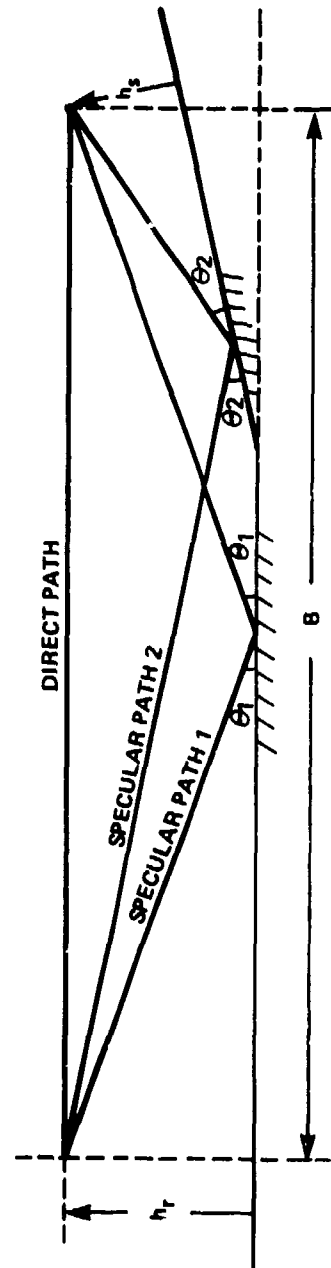
Figure 2. DUAL SPECULAR PATH GEOMETRY

8

If the sources are mounted on light vehicles which can move within the field of view of the APATS, they will probably be no higher than 1.5m. Furthermore, if the vehicles are restricted to speeds less than 18 ms^{-1} (40.5 mph), the baselines may not exceed about 130m if simulation of the specified maximum RV angular rate[*]of 8° s^{-1} is to be performed.

These practical limitations lead to an APATS testing environment characterized by source and receiver heights which are small compared to the baseline separation. Under such conditions, the intervening ground, which will be relatively flat for the airfield test site, should behave as an efficient reflector of radiation from the source to the receiver. If it is assumed that the receiver height is 3m, the source height 1.5m, and the baseline is 130m, the specular grazing angle is:

$$\theta = TAN^{-1}\left(\frac{h_r + h_s}{B}\right) = 1.98^{\circ} \tag{2}$$

The Rayleigh criterion, which, if satisfied, indicates that reflection from a surface is predominantly specular, is given by,[3]

$$\frac{\sigma_h SIN\theta}{\lambda} < \frac{1}{8} \tag{3}$$

in which σ_h is the standard deviation of the surface height. If σ_h is taken to be 6 cm, which is not an unreasonable value for flat terrain, and $\theta = 2^{\circ}$, the left side of (3) is 0.016 and, for the hypothetical test configuration the reflection can certainly be regarded as specular. Under these circumstances, a two-path propagation model should provide an adequate description of multipath interference at the receiver. Specular ray multipath propagation models have been applied with reasonable success to experimental geometries having low grazing angles and ground

* Excludes aircraft dynamics.

9

surfaces consisting of several flat segments between the source and receiver.[4] Figure 2 shows a test configuration for which the ground profile requires that two specular contributions be added to the direct field for a certain range of receiver heights; however, this more complicated geometry will not be considered here.

The total field at a given point in the plane of the receiving array antenna may be considered quite simply as the projection of the vector sum of the direct and specular fields on the array plane. For horizontal polarization, the direct and specular E-fields are colinear and in the array plane, while for vertical polarization, the direct and specular fields are not parallel and projection factors of $\cos \alpha$ and $\cos \theta$ must be employed, as illustrated in Figure 3, to obtain the field component in the plane of the array. The frequencies of the direct and specular fields are very nearly identical at all times, since the relative channel delay, which is typically the order of a nanosecond, is small compared to the shortest modulation period of the carrier. Therefore, the total field at the receiver will not experience "beats" but rather, have an amplitude which depends upon the component field amplitudes, relative path lengths from source to receiver, and Fresnel coefficients.

The phase of the specular field at the receiver position differs from that of the direct field as a consequence of the longer path traversed by the specular field and the phase lag which is experienced by the specular field upon reflection. The Fresnel reflection coefficients, which describe the amplitude and phase change of the incident field upon reflection from a smooth surface, are polarization dependent and are conveniently expressed as complex numbers,
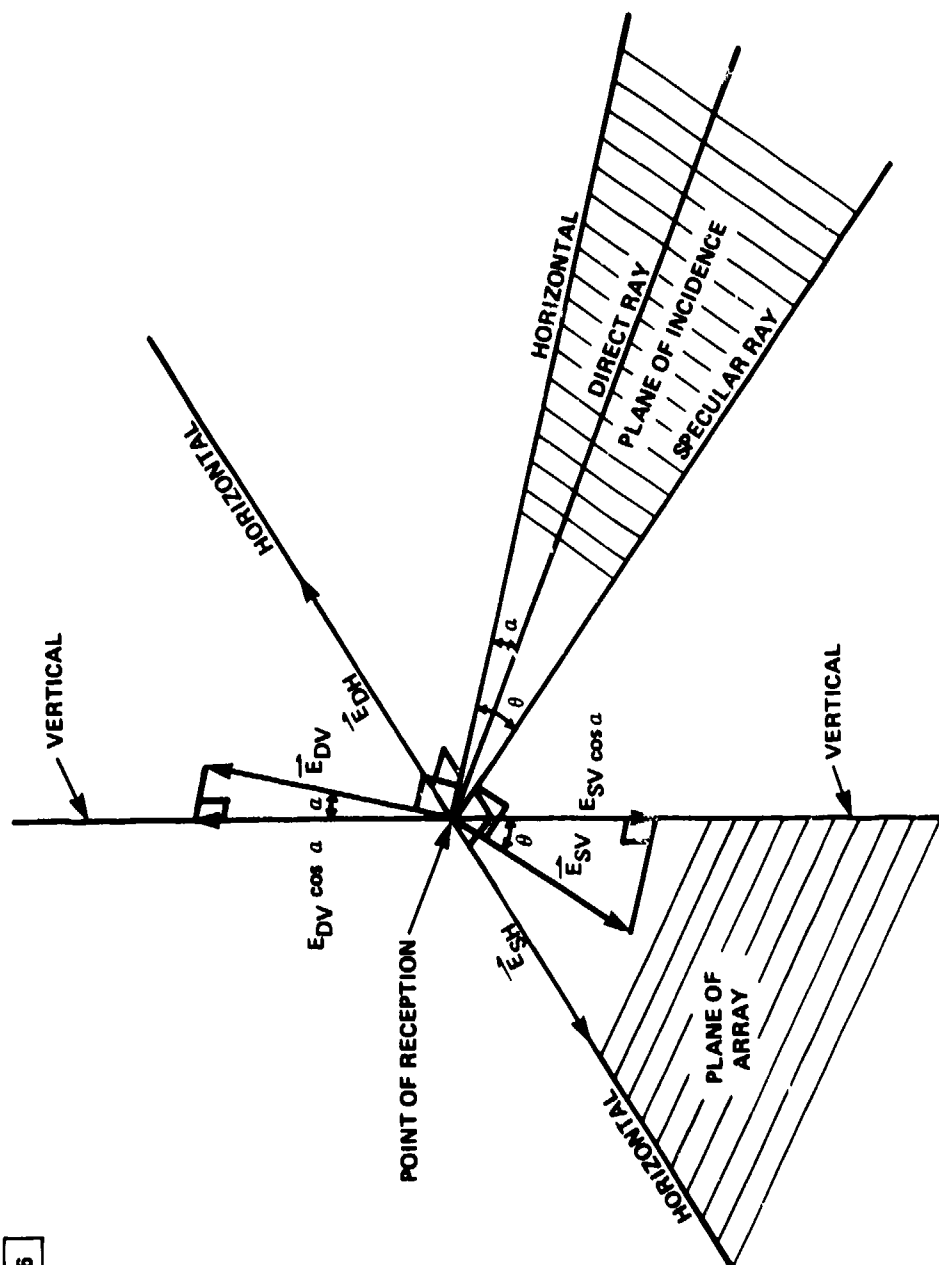
Figure 3. SPATIAL RELATIONSHIP OF DIRECT AND SPECULAR FIELDS IN THE PLANE OF THE ARRAY

Horizontal Polarization: $\rho_{F_H} = \alpha_H e^{-i\phi_H}$ (3a)

Vertical Polarization: $\rho_{F_V} = \alpha_V e^{-i\phi_V}$ (3b)

whose amplitudes, α_H and α_V, and phase lags, ϕ_H and ϕ_V, are functions of grazing angle of incidence, wavelength, surface conductivity and relative dielectric constant. The functional dependence is well established[5] and will not be reproduced here; however, Figures 4 and 5 display the Fresnel coefficient amplitudes and phase lags respectively, for both "average land" ($\sigma = 1.6 \times 10^{-3}$ mho m^{-1}, $\epsilon_r = 10$)[6] and moist ground ($\sigma = 10^{-2}$ mho m^{-1}, $\epsilon_r = 30$)[7]. Note that for vertical polarization the phase lags drop very abruptly from $180°$ to $0°$ at grazing angles which correspond to minima in the vertical coefficient amplitude. For low grazing angles the Fresnel phase lags are nearly $180°$ for both vertical and horizontal polarization.

The path length difference, obtained by geometry from Figure 1 is,

$$\Delta P = [(h_r + h_s)^2 + B^2]^{1/2} - [(h_r - h_s)^2 + B^2]^{1/2}$$ (4)

so that the total phase of the specular field referenced to the direct field is, in radians:

Horizontal Polarization: $\phi_{T_H} = \dfrac{2\pi\Delta P}{\lambda} - \phi_H$ (5a)

Vertical Polarization: $\phi_{T_V} = \dfrac{2\pi\Delta P}{\lambda} - \phi_V$ (5b)

The amplitude of the specular field, relative to the direct field, is given by the product of several factors which are discussed below.

Figure 4. FRESNEL COEFF. AMPLITUDE VERSUS GRAZING ANGLE FOR AVERAGE I AND AND MOIST GROUND

IA-61,905

13
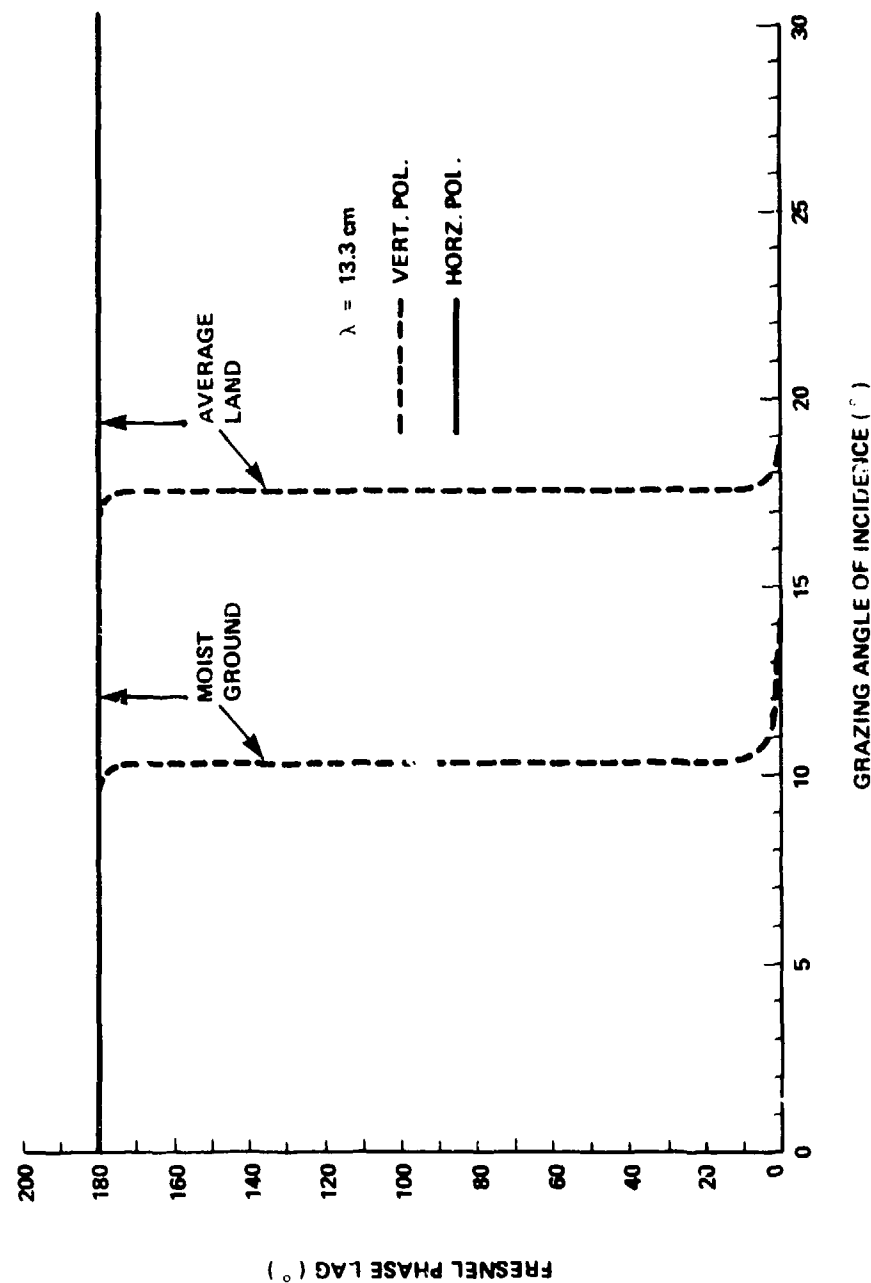
Figure 5. FRESNEL COEFF. PHASE LAG VERSUS GRAZING ANGLE FOR AVERAGE LAND AND MOIST GROUND
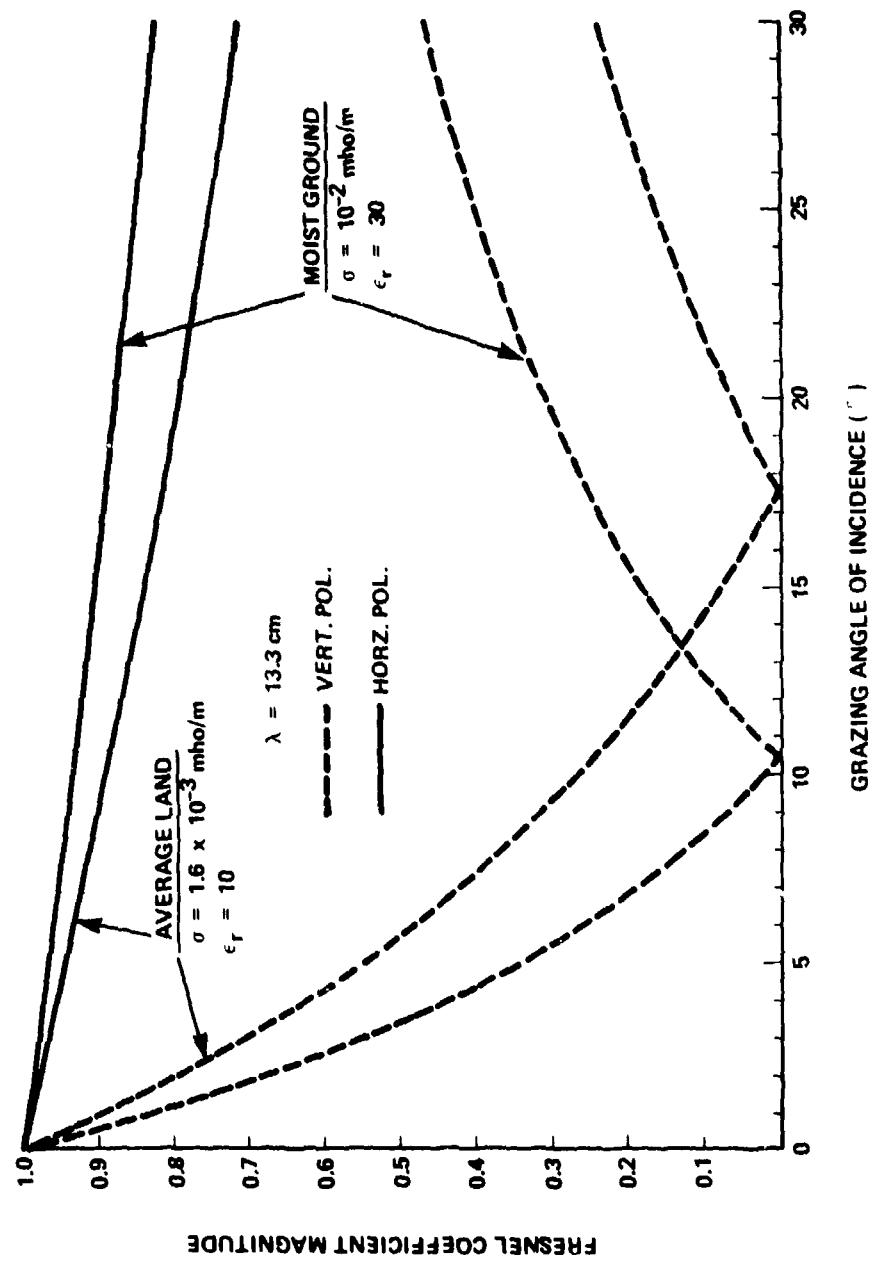
14

The relative gain of the source antenna in the direct and specular ray directions is considered first. For simplicity, it is assumed that the transmitting antenna boresight is horizontal and that the antenna field magnitude has the familiar form,

$$E(\phi, a) = \frac{SIN\left(\frac{\pi a SIN\phi}{\lambda}\right)}{\left(\frac{\pi a SIN\phi}{\lambda}\right)} \qquad (6)$$

in which "ϕ" is the elevation angle and "a" is the aperture vertical dimension. The field amplitude in the specular direction referenced to the direct direction is thus,

$$\rho_A = \frac{SIN\left(\frac{\pi a SIN\theta}{\lambda}\right)}{SIN\left(\frac{\pi a SIN\alpha}{\lambda}\right)} \frac{SIN\alpha}{SIN\theta} \qquad (7)$$

in which θ is the specular grazing angle and α is the direct ray elevation angle as illustrated in Figure 1.

Since the ground surface from which reflection occurs is not perfectly smooth, the power reflected in the specular direction, on the average, is reduced, since incident energy is also scattered in non-specular directions by surface irregularities. The amplitude of the coherent field, which is defined for an ensemble of surfaces whose surface height densities are Gaussian, when normalized to the field amplitude for a perfectly smooth surface, is given by,[8]

$$\rho_R = ex\rho\left[\frac{-8\pi^2\sigma_h^2 SIN^2\theta}{\lambda^2}\right] \qquad (8)$$

which is polarization independent. The Gaussian density assumption gives good agreement with experimental measurements for low surface roughnesses which satisfy the Rayleigh criterion (3).[9] This roughness factor, however, only accounts for the influence of surface roughness in an average sense. Since the scattering surfaces of the test environment are fixed, and, apart from

15

atmospheric effects, the specular field at the receiver will vary in some deterministic manner with grazing angle, the scattered field depends upon the profile of the patch of ground which contributes to the scatter in the receiver direction. For the present analysis, the roughness factor, ρ_R, is simply factored onto the appropriate Fresnel coefficient, ρ_H or ρ_V.

If the ground over which reflection occurs is covered with a blanket of vegetation, such as grass or crops, the absorbing properties of this intervening material must be taken into account. This is most conveniently done by application of a "vegetation factor", designated ρ_v. For low grazing angles ($0.5°$ to $2°$) ρ_v typically has values somewhere between 0.1 and 0.3 at S-band frequencies.[10]

Finally, for vertical polarization, the specular field projection factor ($\cos \theta$) divided by the direct field projection factor ($\cos \alpha$) must be factored onto the total specular amplitude expression, in order to reference the specular field to the direct field.

The propagation factor is a complex number which represents the total field at the receiver position if the direct field is unity. Thus, the resultant field obtained when the direct field has arbitrary phase and magnitude is conveniently found by multiplication by the appropriate propagation factor. The propagation factor is readily expressed in terms of the previously considered variables as the phasor sum of unity (the direct field) and the normalized specular field. Thus,

Horizontal Polarization: $\quad F_H = 1 + \rho_{T_H} e^{i\phi_{T_H}}$ \hfill (9a)

16

$$\text{Vertical Polarization:} \quad F_V = 1 + \rho_{T_V}\, e^{i\phi_{T_V}} \tag{9b}$$

in which,

$$\rho_{T_H} = \rho_\upsilon\, \alpha_H\, \rho_R\, \rho_A \tag{10a}$$

$$\rho_{T_V} = \rho_\upsilon\, \alpha_V\, \rho_R\, \rho_A\, \frac{\cos\theta}{\cos\alpha} \tag{10b}$$

The average power received at a location in space characterized by propagation factors, F_H and F_V is, relative to the direct field alone, given by,

Horizontal Polarization:

$$P_H = \frac{F_H F_H^*}{2} = \frac{1}{2} + \frac{\rho_{T_H}^2}{2} + \rho_{T_H}\, \cos\phi_{T_H} \tag{11a}$$

Vertical Polarization:

$$P_V = \frac{F_V F_V^*}{2} = \frac{1}{2} + \frac{\rho_{T_V}^2}{2} + \rho_{T_V}\, \cos\phi_{T_V} \tag{11b}$$

The propagation factor phase shifts referenced to unity (direct field) are given by,

$$\Phi_H = \sin^{-1}\left[\frac{\rho_{T_H}\, \sin\phi_{T_H}}{(F_H F_H^*)^{1/2}}\right] \tag{12a}$$

$$\Phi_V = \sin^{-1}\left[\frac{\rho_{T_V}\, \sin\phi_{T_V}}{(F_V F_V^*)^{1/2}}\right] \tag{12b}$$

and the total phase along a vertical section of the array as a function of height, h_r, as referenced to the direct field phase at the lowest array position h_1 is,

$$\Phi_{T_H} = \Phi_H + \Phi_d \tag{13a}$$

$$\Phi_{T_V} = \Phi_V + \Phi_d \tag{13b}$$

in which,

$$\Phi_d = \frac{2\pi}{\lambda}\left([(h_1-h_s)^2 + B^2]^{1/2} - [(n_r-h_s)^2 + B^2]^{1/2}\right) \tag{14}$$

is simply the phase difference associated with the direct path
length difference between the bottom of the array and a point above
h_1 at h_r. The horizontal polarization phase relationships are
illustrated in Figure 6.

2.2 USEFUL APPROXIMATIONS

The predictions of the above analysis and relationship between
the variables become clearer if several simplifying approximations
are made. Consider first the path length difference formula of Eq.
(4). If,

$$B \gg h_r + h_s \tag{15}$$

then,

$$\Delta p \cong \frac{2h_r h_s}{B} \tag{16}$$

which shows that, to a good approximation, the path length
difference of the direct and specular channels is directly
proportional to the sender and receiver heights and inversely
proportional to their baseline separation. If the grazing angle is
less than 10° (see Figure 5) both the vertical and horizontal
polarization Fresnel phase shifts are very close to 180°, thus the
power propagation factors of Equations (11a) and (11b) reduce to,

18
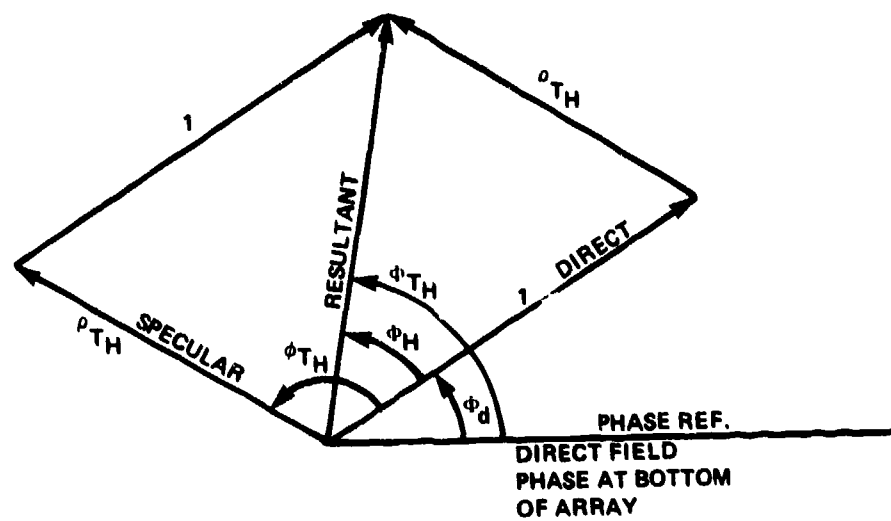
Figure 6. PHASE RELATIONSHIPS FOR DIRECT AND SPECULAR FIELDS

$$P_H = \frac{1}{2} + \frac{\rho_{T_H}^2}{2} - \rho_{T_H} \cos\left(\frac{4\pi h_r h_s}{\lambda B}\right) \qquad \text{(17a)}$$

$$P_V = \frac{1}{2} + \frac{\rho_{T_V}^2}{2} - \rho_{T_V} \cos\left(\frac{4\pi h_r h_s}{\lambda B}\right) \qquad \text{(17b)}$$

and it is evident that minima occur when the argument of the cosine is zero or an integral multiple of 2π radians. Indeed, the power pattern at the receiver will be characterized by a quasi-periodic "lobe structure" which will be evident, for example, when the receiver is moved vertically with the source height and baseline fixed. Under these conditions, the approximate spatial period of the lobes is given by,

$$\frac{4\pi \Delta h_r h_s}{\lambda B} = 2\pi \quad \text{OR,} \quad \Delta h_r = \frac{\lambda B}{2h_s} \qquad \text{(18)}$$

For the example considered earlier, with h_s = 1.5m, B = 130m, and λ = 0.133m, a lobe period of about 5.8m is predicted.

It is instructive to consider the power factor for the case of very small grazing angles and path length differences such that,

$$\lambda \gg \Delta P \qquad \text{(19)}$$

For a smooth flat earth with no vegetation,

$$\rho_{T_H} \cong \rho_{T_V} \cong 1 \qquad \text{(20)}$$

and if condition (19) is satisfied, the cosine may be expressed,

$$\cos\left[\frac{4\pi h_r h_s}{\lambda B}\right] \cong 1 - \left(\frac{4\pi h_r h_s}{\lambda B}\right)^2 \qquad \text{(21)}$$

which yields

$$P_H \cong P_V \cong \left(\frac{4\pi h_r h_s}{\lambda B}\right)^2 \qquad (22)$$

Thus, when the propagation power factor is multiplied by the direct field, which has an inverse square power law, it is seen that the power decreases with the inverse fourth power of the source-receiver separation for propagation paths very close to the surface. This result, which has been noted elsewhere,[12] is only valid for a flat surface, since when earth curvature is introduced diffraction effects and path clearance must be considered.[13] It should be noted that condition (20) is satisfied for a wider range of small grazing angles for horizontal polarization than for vertical polarization as a result of the α_V and α_H dependence on θ, as illustrated in Figure 4.

Equations (13a) and (13b) give the phase of the received field as a function of the vertical array position, h_r. The elevation angle of arrival of a small section of wavefront relative to the array boresight (horizontal) is related to the rate of change of the phase at the vertical position, h_r, by,*

$$\text{SIN } \alpha_r = \frac{\lambda}{2\pi}\left(\frac{-d\phi_T}{dh_r}\right) \qquad (23)$$

Clearly, if the wavefront is not a plane wave, the field's phase gradient across the array will not be constant, and this is especially true when interference with the specular wave occurs. The angle of arrival of the wavefront is then a function of position as indicated by Equation (23).

---

* See Appendix A.

Since the received power is concentrated in the vicinity of the multipath lobe peaks, an approximation to the apparent source elevation can be obtained by calculating the phase gradient in these regions. The total phase, referenced to the direct field phase at the array bottom, in the vicinity of the nth lobe peak, is approximately,

$$\Phi_{T_H} \cong \Phi_d + \left(\frac{\rho_{T_H}}{1 + \rho_{T_H}}\right)\left[\frac{4\pi h_r h_s}{\lambda B} - (2n-1)\pi\right] \tag{24a}$$

$$\Phi_{T_V} \cong \Phi_d + \left(\frac{\rho_{T_V}}{1 + \rho_{T_V}}\right)\left[\frac{4\pi h_r h_s}{\lambda B} - (2n-1)\pi\right] \tag{24b}$$

as illustrated in Figure 7. For lobes which occur at heights corresponding to low grazing angles, ρ_{T_H} and ρ_{T_V} are not very dependent on h_r and can be taken as constant. Therefore, the wavefront in the neighborhood of a lobe peak, which makes the largest contribution to the received power, will appear to be arriving from a direction given by,

$$\alpha_A \cong SIN^{-1}\left[\frac{-\lambda}{2\pi}\left[\frac{d\Phi_d}{dh_r} + \frac{\rho_{T_H}}{1 + \rho_{T_H}}\left(\frac{4\pi h_s}{\lambda B}\right)\right]\right] \tag{25}$$

for the case of, for example, horizontal polarization. The angle, α_A, is only an estimation of the apparent source elevation angle; however, it is instructive to carry this approximation further. If the true elevation angle of the source is small, the arc sin in Eq. (25) can be replaced by its argument:

$$\alpha_A \cong \alpha_{h_r} - \frac{\rho_{T_H}}{1 + \rho_{T_H}}\left(\frac{2h_s}{B}\right) \tag{26}$$

In the above equation, α_{h_r} represents the true elevation angle of the source as given by the phase variation of the direct field alone:

$$\Phi \cong \frac{\rho_T}{\rho_T + 1}\left[\frac{4\pi h_s h_r}{\lambda 8} - \pi (2n - 1)\right]$$

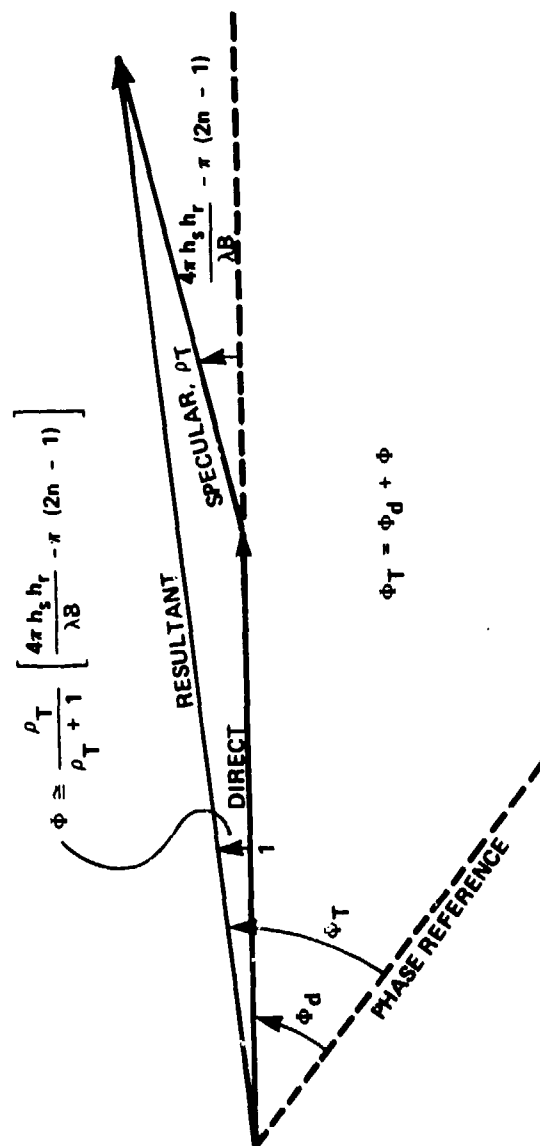$$\frac{4\pi h_s h_r}{\lambda 8} - \pi (2n - 1)$$

$$\Phi_T = \Phi_d + \Phi$$

Figure 7. PHASE APPROXIMATION NEAR nTH LOBE PEAK

$$\alpha_{h_r} = SIN^{-1}\left[\frac{-\lambda}{2\pi}\left(\frac{d\Phi_d}{dh_r}\right)\right]$$ (27)

The phase gradient in Eq. (27) is nearly constant across the array if the source range greatly exceeds the array aperture, as is definitely true if the source is in the far field of the array.

Note that $2h_s/B$ is approximately equal to the angle (in radians) subtended from the array from the source to its image below the surface. The result of Eq. (26) is therefore intuitively satisfying, since the apparent source position moves towards the image position as the relative amplitude of the specular field, ρ_T, increases. If the direct and reflected waves are of equal strength, the apparent source elevation is close to horizontal. It should be stressed that this approximation is only valid for small elevation angles for an antenna which only intercepts one lobe, and neglects power contributions which are not near lobe peaks. The actual tracking errors due to multipath should be far less than indicated by Eq. (26) if two or more lobes are received.

The above analysis has shown how surface reflection can lead to amplitude and phase variations across the face of a phased array antenna. In the following section, the results of specific calculations performed within the framework of the above model for several APATS TAG test configurations and environments are presented and discussed.

SECTION 3

RESULTS AND DISCUSSION

3.1 TEST CONFIGURATION NO. 1: USE OF EXISTING TOWER

APATS TAG tests will be performed at Wright-Patterson AFB near Dayton, Ohio, where the ARIA fleet is based. The existing facilities at the airbase include a 24.25m (79.6 ft.) tower which supports three separate linearly polarized antennas which can transmit S-band telemetry for ARIA pre-mission calibration. In this configuration and those discussed later, it will be assumed that the 30° half-power main beamwidth horn antenna is employed as the source antenna for APATS testing. The location of the tower and operational apron permit a baseline of not less than 400m between the transmitting antenna and ARIA. The intervening ground is very flat and paved with asphalt, but can include some grassy areas depending upon the ARIAs location on the apron.

If the existing tower is employed for APATS TAG tests, tracking simulation is not feasible, since it is not practical to rotate the aircraft. Nevertheless, the tower transmitter may still be used to calibrate the APATS sensitivity against the 2.1m parabolic dish antenna in the ARIA's nose. To investigate the impact of multipath on this type of test, calculations based on the model outlined in Section 2 were performed using the following parameters: source height, 24.25m; baseline, 400m; receiving height range, 1m-5m; surface height standard deviation, 6 cm; wavelength, 13.3 cm; vegetation factor, 1. The transmitting antenna was assumed to have a $\sin^2 x/x^2$ pattern with a 30° half-power beamwidth and horizontal boresight orientation. Since the conductivity and dielectric constant of the asphalt is not known, average land values for these parameters were used.

25

The calculated propagation power factor and total phase of the field versus vertical position in the receiving antenna plane is displayed in Figure 8. Note that the spatial period of the power pattern lobing is about 1.1m in agreement with the result obtained using Eq. (18). The lobing is not as pronounced for vertical polarization, which is not surprising in view of the dependence of the Fresnel amplitudes as illustrated in Figure 4. The lobe pattern does not vary significantly across the receiving plane in the horizontal direction for distances which are small compared to the baseline(e.g. 5%). The parabolic dish, which is laterally offset from the APATS antenna by only several meters, falls within this lobe pattern between the heights of 1.4m and 3.5m, since the 2.1m dish centerline is 2.45m from the ground. Accurate calibration of the array against the dish would require that the array have a 2.1m diameter aperture centered at the same height as the dish, modulo 1.1m, since the power pattern is nearly periodic with a 1.1m period. On the other hand, rough calibration is feasible since both antennas should intercept two lobes and the average power received will be roughly proportional to the aperture area.

The total phase of the RF field versus receiver height is plotted adjacent to the power pattern in Figure 8, and displays interesting features which deserve comment. Although the average total phase follows that of the direct field alone, there are vertical ranges for which the wavefront is nearly linear and rotated by a fixed angle witn respect to the direct field phasefront. For example, a horizontally polarized antenna of 0.8m vertical aperture width or less, if centered at the position of a lobe peak, receives maximum power when it's axis is horizontal, i.e., perpendicular to the local wave or phase front. The true source elevation is 3.2°, so that the hypothetical antenna suffers a pointing error of about 3.2°. Similarly, for vertical polarization, the pointing error for

DIREC

SOURCE H
BASELINE

n_h
o_v

−500

TOTAL POWER (dB)
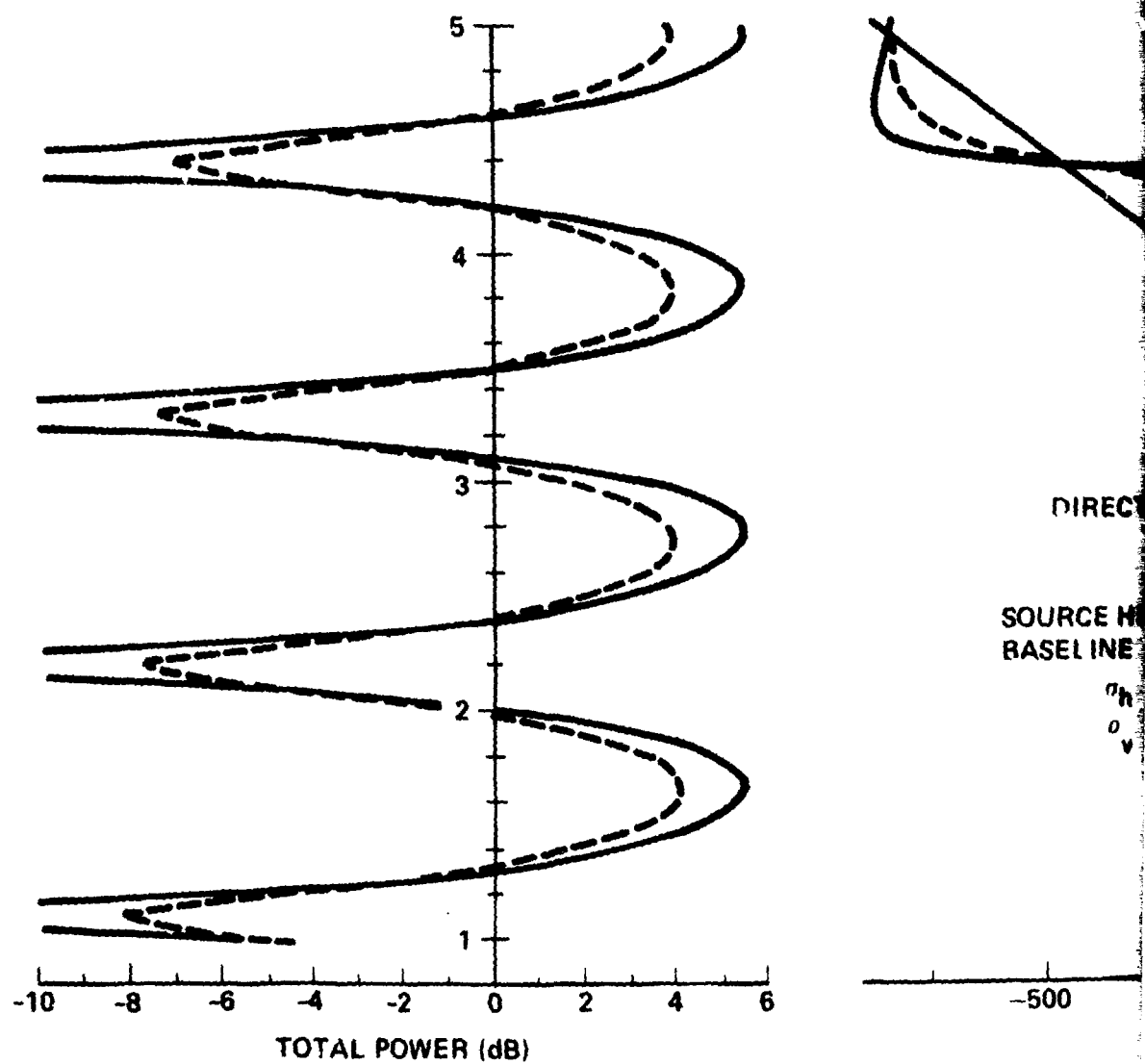
Figure 8. POWER AND PHASE VS. RECEIVER H
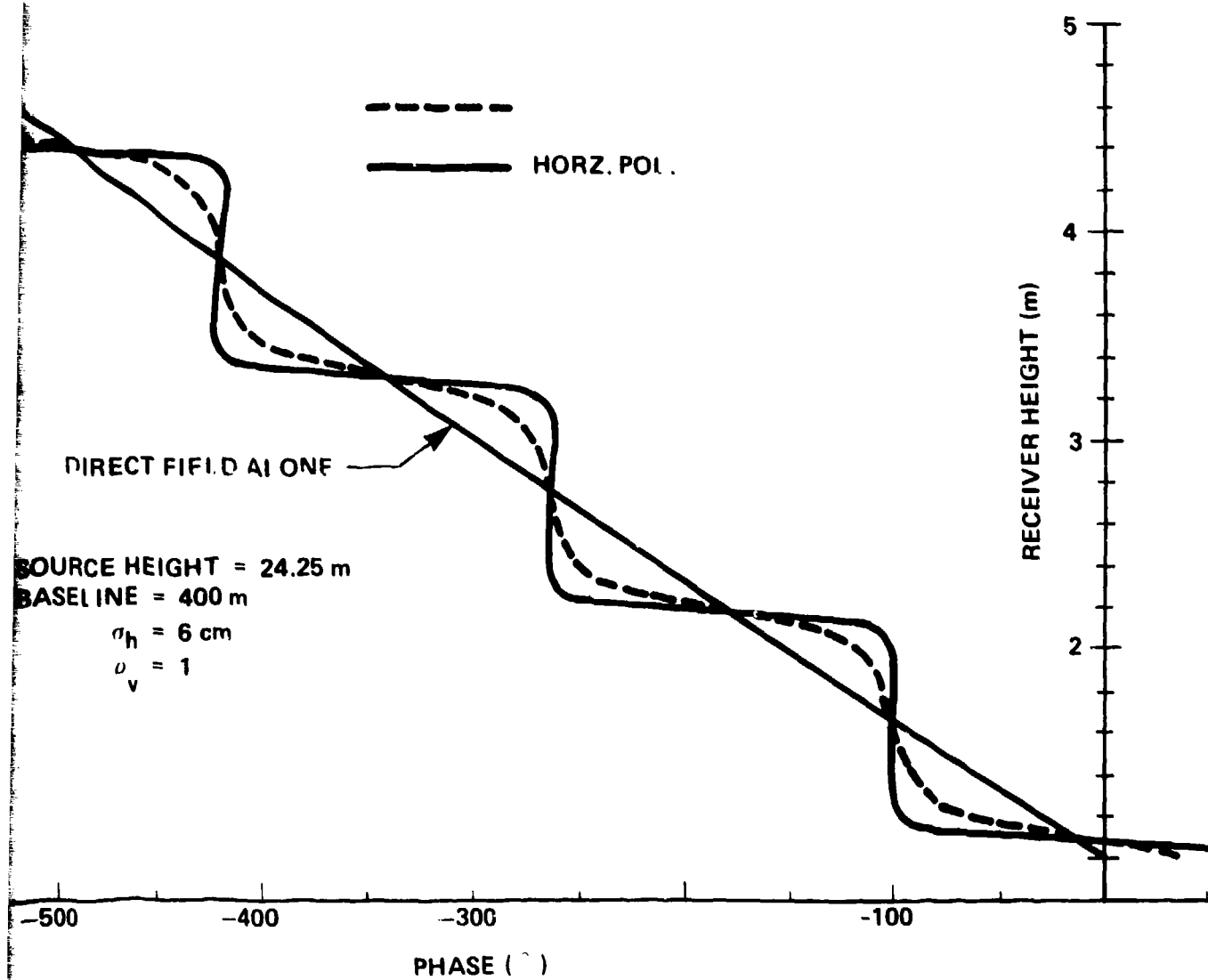
RECEIVER HEIGHT – TOWER TO APATS; NO VEGETATION
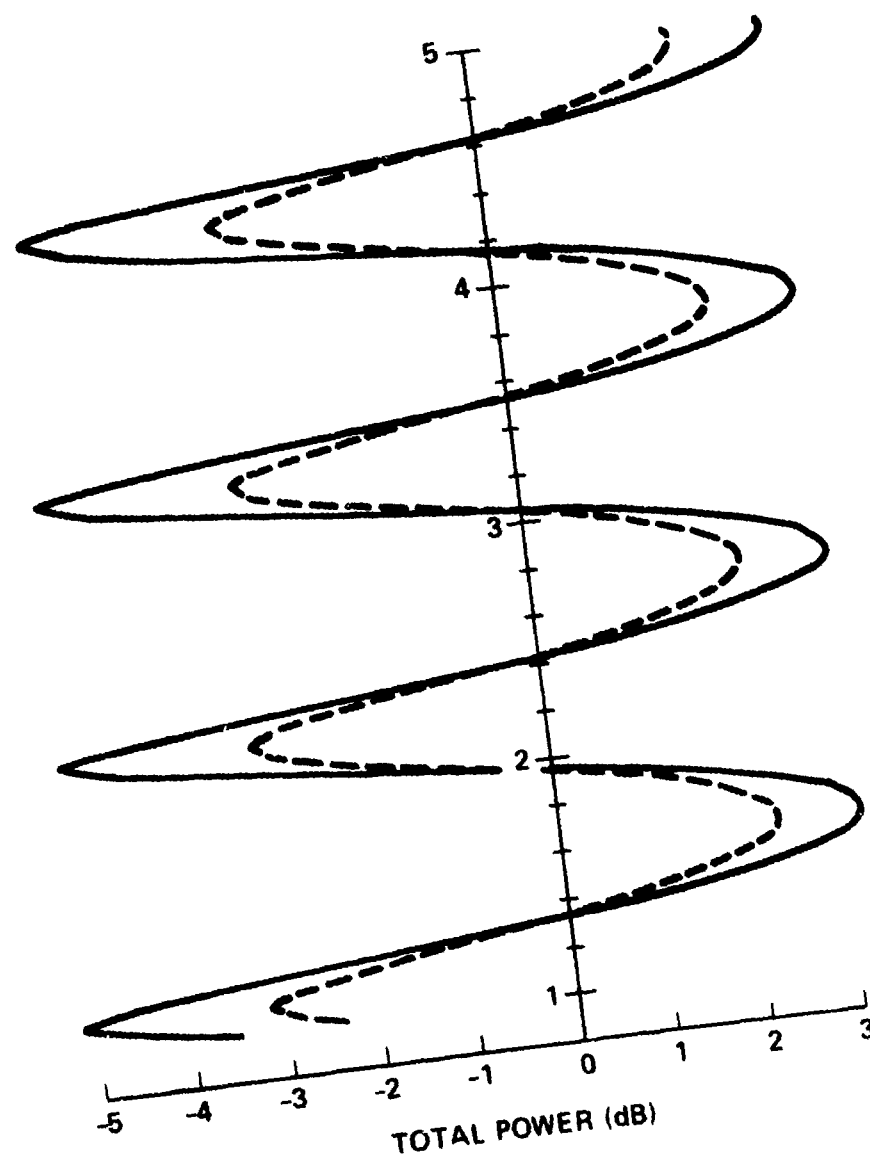
SOURCE H
BASELINE

$_0$h
$_0$
$_v$

−600   −500

Figure 9. POWER AND PHASE VS. RECEIVER HE

TOTAL POWER (dB)

VERT. POL. ----

HORZ. POL. ———

DIRECT FIELD
ALONE

SOURCE HEIGHT = 24.25 m
BASELINE = 400 m

σ_h = 6 cm

υ_v = 0.5

PHASE (°)

RECEIVER HEIGHT (m)

RECEIVER HEIGHT – TOWER TO APATS; VEGETATION

29

a somewhat smaller antenna would be 2.5^O. Thus, for receiving antennas smaller than the lobe periodicity and centered on a lobe peak, the source will appear to be displaced downward, towards its image below the surface, by an angular distance with increases with the strength of the reflected field. The approximate value of the pointing error is indicated by Eq. (26) if the grazing angle is small ($\sim$0.2 rad or less). For larger aperture receiving antennas, the phase variations are averaged out and pointing errors are less significant.

The next test scenario considered is identical to the previous one, save for the vegetation factor, which is assumed to be 0.5. The 0.5 value represents an educated guess, since values of 0.1 to 0.3 are typical;[10] however, the vegetation at the airfield test site is likely to be sparse, and therefore not as effective an absorber of microwaves as suggested by the typical values.

The propagation power factor and total phase versus receiver height is shown in Figure 9. As anticipated, the use of the smaller vegetation factor reduces the excursions of both the power factor and total phase deviations, but does not effect their periodicity, which is a function of the geometric parameters of the test configuration and the wavelength (Eq. 18). The power factor minima are far less severe, while the maxima are reduced by almost a factor of two. Elevation angle pointing errors for small (0.6m or less) receiving antennas located at lobe peak positions are approximately 2.0^O and 1.4^O for horizontal and vertical polarizations, respectively. If the receiving antennas are large enough to include two or more lobes, the phase deviations will average out and the pointing error is smaller.

31

Both of these test scenarios feature a 400m baseline. This particular value was chosen, since it represents the shortest baseline possible if the ARIA is to remain on the operational apron at the airfield test site. Longer baselines, although possible, are not desirable since, by Eq. (18), the lobe spatial period increases linearly with baseline. As indicated earlier, when the lobe period becomes comparable to or greater than the array or dish antenna vertical aperture dimension, pointing errors will be more serious, and if the two antennas are not at the same height, they may be sampling areas of greatly different field strength. Test configurations characterized by lobe periods which are small compared to the receiving antenna aperture will not be seriously degraded by multipath interference.

3.2 TEST CONFIGURATION NO. 2: SOURCES ON LIGHT GROUND VEHICLES

In order to test the APATS tracking capability, it is necessary for the source(s) to move within the field of view of the phased array antenna. It has been suggested that a transmitting antenna be mounted upon a light vehicle, such as a jeep, which may be driven across the APATS field of view to exercise both acquisition and tracking. As pointed out near the beginning of Section 2, the antenna-source baseline should exceed 60m in order to remain in the far field of the receiving antenna, and should be less than 130m, in order to permit simulation of an 8° s^{-1} angular rate at a vehicle speed less than 18 ms^{-1} (40.5 mph). It is estimated that an antenna mounted upon a jeep will be 1.5m (5 ft.) above the ground.

Test configuration 2 is characterized by the following parameters: source height, 1.5m; baseline, 130m; receiver height range, 1m to 5m; surface height standard deviation, 6 cm; wavelength, 13.3 cm; and vegetation factor, 1. The source antenna,

32

as in the previous configurations, was assumed to have a 30° half-power beamwidth and horizontal boresight orientation. The conductivity and relative dielectric constant values for average land[6] were used.

In Figure 10 the power factor and total RF phase of the field at the receiving position are displayed as a function of height. For this test configuration, the lobe spatial periodicity is about 5.8m, and both the dish and APATS antennas lie mainly within the positive portion of the first lobe. Since the dish is situated between 1.4m and 3.5m, the array would have to occupy the same height range or the range of 2.3m to 4.4m, which covers a portion of the first lobe nearly symmetrical to that covered by the dish, if accurate relative sensitivity measurements are to be performed. On the other hand, if accurate sensitivity calibration is not important, this test configuration should be satisfactory for rough measurements and tracking tests, since neither the array or dish are in an interference minimum. Note that if a baseline of 60m were employed, a minimum would occur at a receiver height of about 2.7m, which is the approximate array position. Thus, short baselines should be avoided and an operational vehicle maneuvering range of 100m to 150m is suggested if sources carried by ground vehicles are employed for source mobility.

The apparent source elevation angle can be determined for configuration 2 by calculation of the average vertical phase gradient over the antenna aperture in accordance with Eq. (23). For the dish situated between 1.4m and 3.5m, the source will appear to be at an elevation of -1.1^O and -1.0^O for horizontal and vertical polarization, respectively, rather than the true elevation of -0.4^O. The angular error of 0.6^O to 0.7^O is not significant when compared to the dish half-power beamwidth of $\sim 4^O$. Similarly, for an array

33

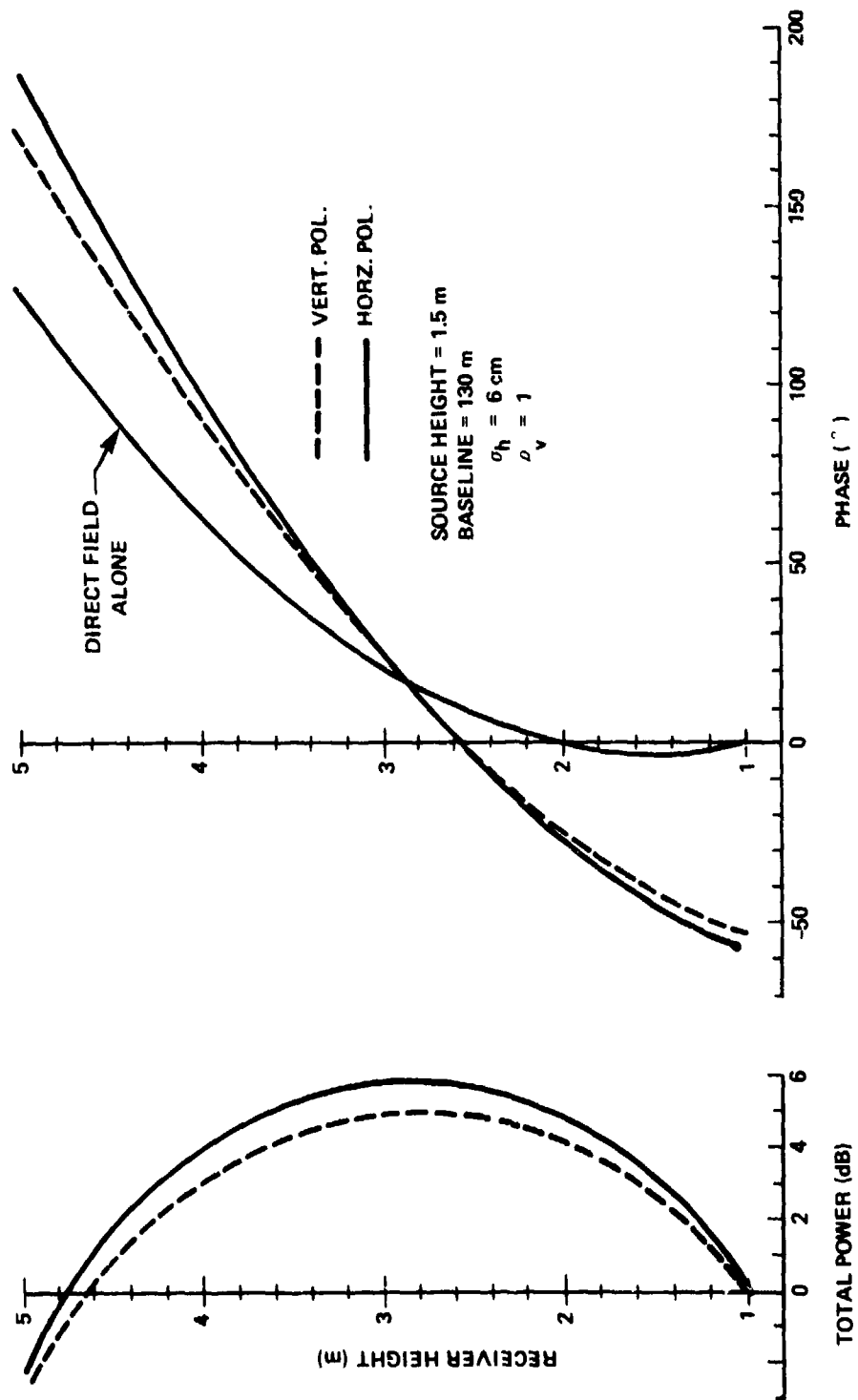Figure 10. POWER AND PHASE VS. RECEIVER HEIGHT – GROUND SOURCE TO APATS: NO VEGETATION

IA-61,900

34

situated a bit higher between 2.3m and 4.4m the source appears to be at an elevation of -1.45° and -1.35° for horizontal and vertical polarization, respectively, rather than the correct value of -0.8°. Again the angular errors are small compared to the array beamwidth. It should be noted that accurate RV tracking is not an APATS requirement, but rather, the purpose of the tracking is to insure that the RV signal is received with satisfactory gain. Since lobing of the field strength is only significant over the vertical antenna dimension, azimuthal tracking errors should be negligible.

The next test environment considered is identical to the previous one except for a vegetation factor of 0.5 to account for absorption by grass covered ground. As is seen in Figure 11, the reduction in the "bounce signal" by vegetative absorption reduces the positive excursion of the first lobe by about 3 dB. In addition, the average phase front gradient indicates source elevation errors of only 0.3° to 0.4° for both horizontal and vertical polarization if the receiving antenna locations used for the previous case are assumed. Clearly, APATS TAG testing over grassy terrain will mitigate multipath interference.

3.3 TEST CONFIGURATION NO. 3: GRAZING ANGLE OPTIMIZATION

The grazing angle of incidence for which the vertical polarization Fresnel coefficient is minimized is referred to as the Brewster angle. From an examination of Figure 4, it is evident that the Brewster angles for average land and moist ground are 17.5° and 10.5°, respectively. If the test configuration geometry is contrived to cause the specular ray from the source to the center of the array to graze the ground at the Brewster angle, specula. reflection will be nearly eliminated for vertical polarization.
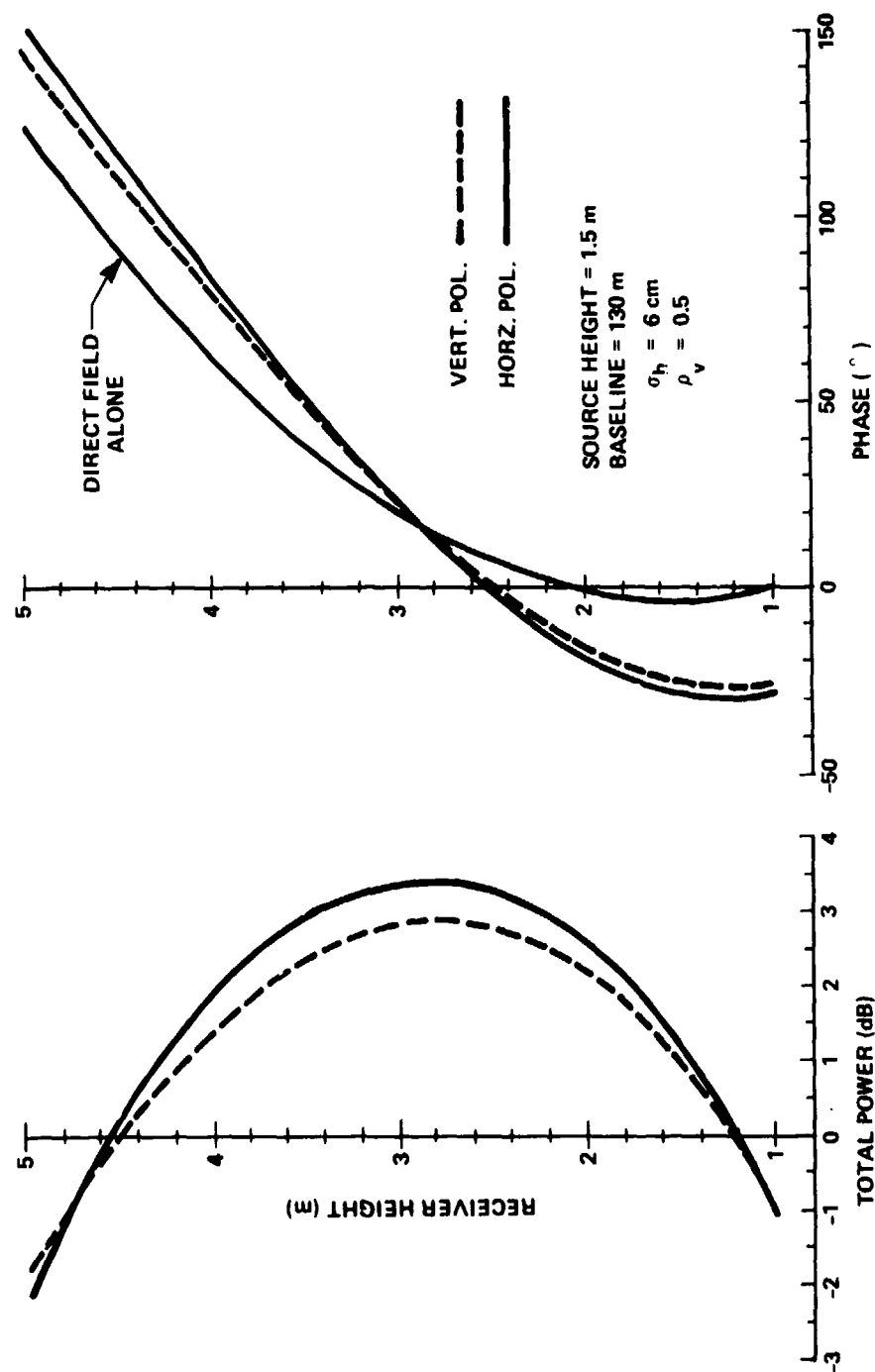
35

Figure 11. POWER AND PHASE VS. RECEIVER HEIGHT — GROUND SOURCE TO APATS; VEGETATION

IA-61,899

36

If the source is at a line-of-sight distance "D" from the array center which is at height h_r, and the Brewster angle is θ_B, the required source height and baseline for Brewster angle optimization are, respectively,

$$h_S = SIN\ \theta_B \left[\frac{h_r}{TAN^2(2\theta_B)} - \frac{h_r^2}{SIN^2\theta_B} + D^2 \right]^{\frac{1}{2}} - h_r COS(2\theta_B) \qquad (28)$$

$$B = \frac{h_r + h_S}{TAN\ \theta_B} \qquad (29)$$

Tables 1 and 2 give calculated values of h_S and B for various combinations of receiver height and source-receiver line-of-sight separation, for grazing angles of 17.5^O and 10.5^O, respectively. The indicated source heights and baselines would require the mounting of the source antenna on a nearby building several stories high or tower if this grazing angle optimization technique for vertical polarization is to be used. Clearly, this configuration would be most suitable for static calibration of the array sensitivity.

3.4 TEST CONFIGURATION 4: LARGER GRAZING ANGLES

If the transmitting antenna is placed at a height which is some significant fraction of the test configuration baseline, multipath effects will not have a significant impact on the test results. Basically, this is due to the high directivity of the receiving antennas. A simple example suffices to illustrate this point. Consider a source at a height of 20m which has a baseline separation of 60m from a receiver at a height of 3m. The angular separation between the direct and specular rays is 36.8^O, which puts the specular ray far outside the main beam of the receiving antenna. The propagation power factor lobe structure for this geometry is displayed in Figure 12, which shows that the receiving antenna
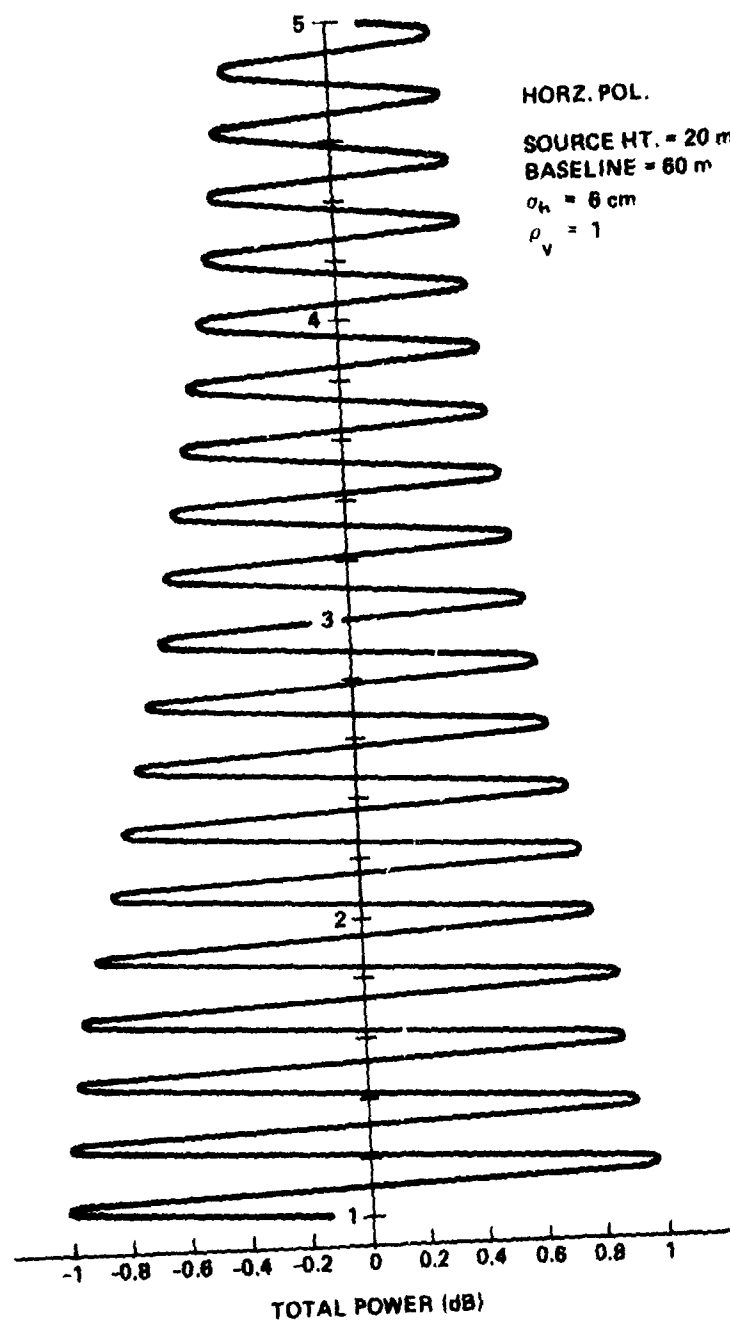
37

HORZ. POL.

SOURCE HT. = 20 m
BASELINE = 60 m
σ_h = 6 cm
ρ_v = 1

TOTAL POWER (dB)

IA-61.911

Figure 12. POWER VARIATION FOR HYPOTHETICAL TOWER CONFIGURATION

38

aperture will encompass many lobes of the interference pattern and will effectively perform an average over these quasi-periodic. perturbations.

3.5 TEST CONFIGURATION 5: SPECIALLY DESIGNED TOWER

A possible APATS test configuration which has considerable merit from a technical standpoint has been suggested.[14] The source antenna support structure would consist of a tower with an arm or arms which pivot about a horizontal axis after the fashion of a windmill. The ends of the arms would be fitted with the source antennas which would rotate as the arms are rotated. APATS tracking of two (one arm) or four (two perpendicular arms) sources simultaneously could be exercised with this arrangement by simply rotating the arms in a plane predominantly perpendicular to the array boresight. Since the linearly polarized source antennas are rigidly fixed to the arms, the transmitted field's plane of polarization will also rotate, providing a test of APATS polarization diversity. On the other hand, if the sources were nutated, the source antenna polarization plane would be preserved.

A tower 30m high with arms having a 10m radius would provide a sweep through ~4 APATS beamwidths in both azimuth and elevation for a 60m baseline separation. Furthermore, the tower would be high enough to greatly reduce multipath interference. A rotation rate of ~9 RPM would be necessary to provide the maximum required $8^{\circ}s^{-1}$ angular rate simulation. The major drawback of this testing procedure is the effort and expense required to locate or produce a suitable source antenna platform.

3.6 TEST CONFIGURATION 6: AIRBORNE SOURCES

Thus far, consideration has been limited to ground-based sources; however, there is no reason why airborne sources, carried by light planes, helicopters, or balloons, cannot be employed. If the elevation angle of the source with respect to the array is maintained at 15° or greater, multipath effects should be negligible.

The above list of configurations is not intended to be exhaustive, but merely to illustrate several viable test options and the anticipated impact multipath propagation has on each.

REFERENCES

1. M. I. Skolnik, <u>Introduction to Radar Systems</u> (McGraw-Hill, 1980) p. 229.

2. See, for example, M. W. Long, <u>Radar Reflectivity of Land and Sea</u> (Lexington Books, Lexington, MA, 1975) p. 39.

3. P. Beckmann and A. Spizzichino, <u>The Scattering of Electromagnetic Waves from Rough Surfaces</u> (MacMillan Co., N.Y., 1963) p. 10.

4. U. H. W. Lammers and D. T. Hayes, "Multipath Propagation over Snow at Millimeter Wavelengths," RADC-TR-80-54, Feb. 1980, AD A 087 747.

5. For a comprehensive treatment of Fresnel coefficients, see, H. R. Reed and C. M. Russel, <u>Ultra High Frequency Propagation</u> (John Wiley and Sons, N.Y., 1953) p. 83-99.

6. M. W. Long, <u>Radar Reflectivity of Land and Sea</u> (Lexington Books, Lexington, MA, 1975) p. 107.

7. D. E. Kerr, <u>Propagation of Short Radio Waves</u> (McGraw-Hill, 1951) p. 398.

8. Op. cit. 3, p. 246.

9. E.g., C. I. Beard, "Coherent and Incoherent Scattering of Microwaves from the Ocean," IRE Trans., Vol. AP-9, Sept. 1961, p. 474, Figure 2.

10. D. K. Barton, "Low-Altitude Tracking Over Rough Surfaces, I: Theoretical Predictions," EASCON 79, Vol. 2, Oct. 1979, p. 226.

11. Examples of such lobe structures are calculated and illustrated in Ref. 2, p. 107-110.

12. W. C. Jakes, Ed., <u>Microwave Mobile Communications</u> (John Wiley and Sons, N.Y., 1974) p. 83.

13. See for example, <u>Reference Data for Radio Engineers</u> (Howard Sams and Co., Indianapolis, Indiana, 1975) p. 28-15 to 28-17.

14. Private communication, J. Orlowski, ARIA Engineering, Wright-Patterson AFB, Dayton, Ohio

APPENDIX

Consider an array which lies in a vertical plane. Cartesian basis vectors $\hat{y}$ and $\hat{x}$ lie in the plane of the array with $\hat{y}$ vertical, while $\hat{z}$ lies along the boresight. A point in the array plane has position vector $\vec{R}$ with respect to the origin at the array center,

$$\vec{R} = x \hat{x} + y \hat{y} \tag{30}$$

while a plane wave incident upon the array is characterized by its propagation vector $\vec{k}$, which is perpendicular to the wavefront and has, by definition, the magnitude,

$$|\vec{k}| = \frac{2\pi}{\lambda} \tag{31}$$

The components of $\vec{k}$ in the array coordinate system are conveniently expressed in terms of $\vec{k}$'s direction cosines, $\cos\alpha$ and $\cos\beta$, with respect to the $\hat{x}$ and $\hat{y}$ axes, respectively:

$$\vec{k} = k_x \hat{x} + k_y \hat{y} = \frac{2\pi}{\lambda} \left[\cos\alpha \, \hat{x} + \cos\beta \, \hat{y} \right] \tag{32}$$

The phase of the wavefront at the array point (x, y) as referenced to the origin is given by the dot product of the propagation and position vectors:

$$\phi(x, y) = \vec{k} \cdot \vec{R} = \frac{2\pi}{\lambda} \left[x \cos\alpha + y \cos\beta \right] \tag{33}$$

The components of the phase gradient in the array plane are therefore,

$$G_x = \frac{\partial \phi(x, y)}{\partial x} = \frac{2\pi}{\lambda} \cos\alpha \tag{34a}$$

$$G_y = \frac{\partial \phi(x, y)}{\partial y} = \frac{2\pi}{\lambda} \cos\beta \tag{34b}$$

43

Now assume a general phase function defined on the array plane.

$$\phi \equiv \phi(x, y)$$

The gradient of the phase function can be identified with a <u>local</u> propagation vector whose direction cosines are,

$$\cos \alpha_1 = \frac{\lambda}{2\pi} \left[\frac{\partial \phi}{\partial x}\right]_{x_1} \tag{35a}$$

$$\cos \beta_1 = \frac{\lambda}{2\pi} \left[\frac{\partial \phi}{\partial y}\right]_{y_1} \tag{35b}$$

If the phase gradient component along $\hat{x}$ (horizontal) is negligible, $\alpha = 90^{\circ}$ and the local propagation vector lies in a vertical plane with elevation angle γ, for which, by geometry,

$$\sin \gamma_1 = -\cos \beta_1 \tag{36}$$

so that,

$$\sin \gamma_1 = -\frac{\lambda}{2\pi} \left[\frac{\partial \phi}{\partial y}\right]_{y_1} \tag{37}$$

which is essentially the same as Equation (23).